Hindawi
International Journal of Aerospace Engineering
Volume 2020, Article ID 9193740, 12 pages
https://doi.org/10.1155/2020/9193740

Research Article

The Eu:CROPIS Mass Property Campaign: Trimming a Spin-Stabilized Compact Satellite for a Long-Term Artificial Gravity Experiment

Fabian Orlowski-Feldhusen,[1] **Sebastian Kottmeier**,[1] **Ansgar Heidecker**,[1] **Olaf Mierheim**,[2] **Oliver Kolakowski**,[3] **and Robert Klöpper**[3]

[1]*DLR, Institute of Space Systems, Robert-Hooke-Str. 7, 28359 Bremen, Germany*
[2]*DLR, Institute of Composite Structures and Adaptive Systems, Lilienthalplatz 7, 38108 Braunschweig, Germany*
[3]*Resonic GmbH, Schwarzschildstr. 1, 12489 Berlin, Germany*

Correspondence should be addressed to Fabian Orlowski-Feldhusen; fabian.orlowski@dlr.de

Received 25 February 2020; Revised 16 September 2020; Accepted 5 October 2020; Published 2 November 2020

Academic Editor: Franco Bernelli-Zazzera

Eu:CROPIS (Euglena Combined Regenerative Organic Food Production in Space) is the first mission of DLR's compact satellite program. The launch of Eu:CROPIS took place on December 3rd in 2018 on-board the Falcon 9 SSO-A mission. The satellite's primary payload Eu:CROPIS features a biological experiment in the context of closed loop coupled life support systems. The Eu:CROPIS satellite mission uses spin stabilization along its $\boldsymbol{Z}$-axis to provide defined acceleration levels for the primary and secondary payloads to simulate either a Moon or Mars gravity environment. For the payload performance, it is vital to achieve a minimum deviation between spacecraft $\boldsymbol{Z}$-axis and the major moment of inertia (MoI) axis to minimize the offset of the envisaged acceleration levels. Specific moment of inertia ratios between the spin- and minor axes had to be maintained to allow the attitude control system to keep the satellite at a stable rotation despite environmental disturbances. This paper presents the adaptive and flexible trimming strategy applied during the flight model production, as well as the mass property measurement acceptance campaign and the respective results.

1. Introduction

Eu:CROPIS is the first satellite of the German Aerospace Center (DLR) compact satellite program. Compact satellites are designed and developed for their specific scientific purpose by the DLR Institute of Space Systems in Bremen. Eu:CROPIS is a spin stabilized small satellite placed into a circular low Earth Sun synchronous orbit at an altitude of 580 km and an inclination of 97.8 deg. It was launched on-board a Falcon 9 on 3rd December 2018 in the frame of the Spaceflight Industries SSO-A mission and was operated for about one year [1, 2].

The primary payload Eu:CROPIS is a closed loop coupled life support system and is also the name giver for the whole satellite mission. Tomato seeds in two greenhouses located at the outer cylinder wall of the primary payload will germinate, grow, and produce food and oxygen under Moon and Mars gravitational levels achieved by specific rotation rates (Figure 1(a)). To provide the payloads with homogenous gravity, the deviation between actual rotation axis and spacecraft structural coordinate frame (SCF) Z-axis has to be minimized (Figure 1(b)).

The Attitude and Orbit Control System (AOCS) utilizes a magnetic spin stabilization concept along the major moment of inertia axis [3, 4]. The key idea behind this concept is the fact that only a spin around the major moment of inertia axis is passively stable. In addition, magnetic torquers are not limited by fuel consumption or mechanical degradation. Three magnetic torquers are arranged orthogonally and provide a torque by the interaction between the geomagnetic field and their own magnetic field. They can spin up the satellite up to ~31 rpm, which is the equivalent of Martian gravity at

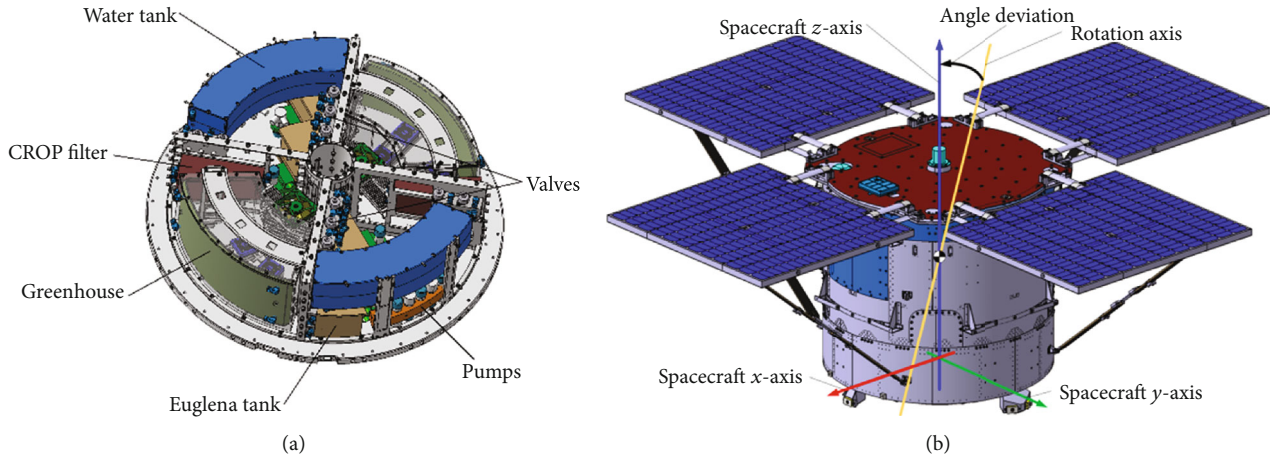

Figure 1: P/L1 and rotation axis deviation.

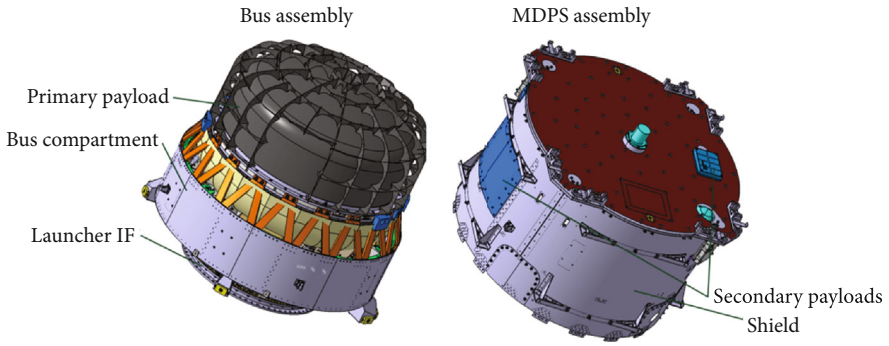

Figure 2: Major assemblies.

a reference radius of 0.35 m. During nominal operation, any angular rate between ~5 and ~31 rpm can be chosen by the operator. Alongside the primary payload Eu:CROPIS, the satellite carries two NASA Ames Powercell Enclosures, two Radiation Measurements in Space (RAMIS) radiation detectors, and the SCalable On-boaRd computer development (SCORE). Detailed information on the mission, subsystems, and payloads can be found in the system overview of reference [1, 2].

The satellite is divided into two main assemblies: the bus assembly containing most of the avionic systems and also the primary payload; the Micrometeroid Debris Protection Shield (MDPS) section containing most of the secondary payloads as well as smaller electronic devices (Figure 2). The solar panels are integrated after structural mating of the two main assemblies.

Eu:CROPIS weighs 234 kg, and its dimensions in launch configuration are approximately $1.1\,\text{m} \times 1.1\,\text{m} \times 1.1\,\text{m}$. When the four solar panels are deployed, Eu:CROPIS' dimensions increase to approximately $2.9\,\text{m} \times 2.9\,\text{m} \times 1.1\,\text{m}$.

Three configuration statuses are passed through during the mission (Table 1):

(1) Launch configuration (Figure 3(a))

(2) Stowed flight configuration (Figure 3(b))

(3) Deployed flight configuration (Figure 3(c))

Table 1: Nominal configuration statuses.

Satellite configuration	Separation system	Solar panels
Launch configuration	Launch configuration	Stowed
Stowed configuration	Flight configuration	Stowed
Deployed configuration	Flight configuration	Deployed

The status of the solar panels and of the separation system is described by the different satellite configurations. There are two possible statuses for the solar panels and for the separation system: The solar panels can be stowed or deployed, and the separation system can be in launch or in flight configuration. The transition ring as well as the complete separation system is attached to the satellite in launch configuration. Only the upper part of the separation system remains attached to the satellite in flight configuration.

In addition to the nominal deployed flight configuration, 14 failure case configurations are possible in which one or more solar panels fail to deploy. Mass properties of all possible configurations have to be calculated.

2. Requirements, Challenges, and Constraints

Requirements from the biological primary payload, AOCS and launcher have to be respected. The applicability of these requirements depends on the configuration and mission

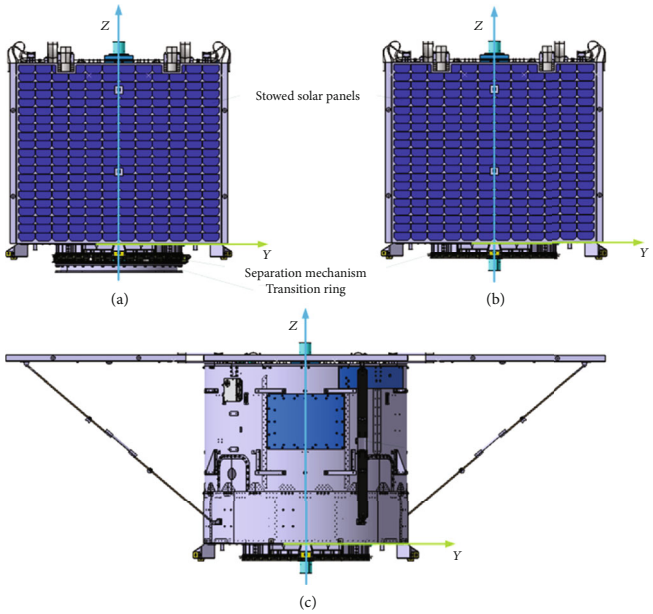

Figure 3: Nominal configurations during the mission.

status, e.g., some requirements are only applicable for the launch configuration (Table 2).

The biological payloads demand for homogeneous artificial gravity within their experiment compartments. The maximum allowable gravity gradient along the outer wall of the payload compartment is 0.05 g (RE-PL-1).

To meet this requirement, the deviation of the CoM position (Δr_{CoM}) and the major MoI axis angle (α) w.r.t. SCF Z -axis can be traded against each other. Figure 4(a) shows the basic geometry of the payload compartment, where the greenhouses are located on the outer cylinder walls. By applying some trigonometry, Figure 4(b) can be generated. This shows the limiting values of Δr_{CoM} and α for a gradient acceleration of 0.05 g along the greenhouse wall. The red line marks the maximum value of either the center of mass shift or the major moment of inertia axis angle at a nominal rotation speed of ~31.16 rpm.

Five requirements from the AOCS have to be fulfilled to allow a stable control of the satellite. First, the rotation axis shall be the major principal axis (RE-AOCS-1), and second, the maximum MoI M_{max} shall be less than 50 kgm^2 (RE-AOCS-2). Third, the ratio between the major principal moment and the minor principal moment $M_{\mathrm{max}}/M_{\mathrm{min}}$ shall be in between 1.1 and 1.2 (RE-AOCS-3). Fourth, the two minor principal moments M_2 and M_3 shall not deviate more than 5% from each other (RE-AOCS-4). Fifth, the angle between solar array normal and sun direction shall be less than 5 degrees during nominal operations (RE-AOCS-5). AOCS requirements 1-4 ensure a stable control with sufficient agility of the satellite whereas requirement 5 ensures sufficient power generation and homogenous artificial gravity.

Three requirements from the launch provider apply. First, the mass of the flight model (FM) and mass model shall be below 250 kg (RE-LP-1). Second, FM's and mass model's lateral CoM offset has to be below 12 mm (RE-LP-2). Third, FM's and mass model's axial CoM offset has to stay below 445 mm (RE-LP-3).

Table 2: Requirement applicability matrix.

	Launch	Stowed	Deployed
RE-PL-1			X
RE-AOCS-1		X	X
RE-AOCS-2		X	X
RE-AOCS-3			X
RE-AOCS-4			X
RE-AOCS-5			X
RE-LP-1	X		
RE-LP-2	X		
RE-LP-3	X		

Derived from the satellite requirements, requirements concerning the test facility properties are defined. The accuracy of the test rig shall be high enough to judge if requirements like the ratio of the two minor moments of inertia are within its limit; this means the measurement uncertainty shall be lower than 2.5%. An easy, safe, and quick handling of the satellite on the test rig is preferable. For the structural model (SM), Biosafety level 1 (BSL-1) was not an issue as it did not contain any genetically modified organisms (GMOs), but for the flight model (FM), it was. The test facility shall be therefore already BSL-1 certified or it shall be possible to certify it to BSL-1. As the BSL-1 certification is costly, a facility being already certified is preferred. To reduce the logistic effort and its corresponding risk for damages on the FM, the test facility shall be in the vicinity of the integration laboratory.

3. FM Mass Property Test and Trimming Strategy

The FM mass property campaign started with the SM mass property measurement (MPM) end of 2015. Mass property test results of the SM did not satisfy accuracy requirements in terms of MoI for Eu:CROPIS as the chosen test center is dimensioned for much heavier satellites. For the SM, a heavy adapter had to be used which was in the same mass region as the SM itself. The accuracy was not high enough to state if previously mentioned requirements were met. Therefore, a different test facility was chosen for FM testing which can deal with all previous mentioned test facility requirements.

Despite the relatively low accuracy of the SM MPM and also configuration differences between SM and FM, the need for trim measures on the FM became obvious. During the SM MPM test, the stowed and deployed configurations had been tested. The angle between major principal axis and SCF Z -axis was far above its five-degree limit. In addition, the difference between the major moment of inertia and the second moment of inertia was below 0.1 kgm^2 in stowed configuration; this could result in an uncontrollable behaviour of the satellite. Also, the ratio of the two minor principal MoIs

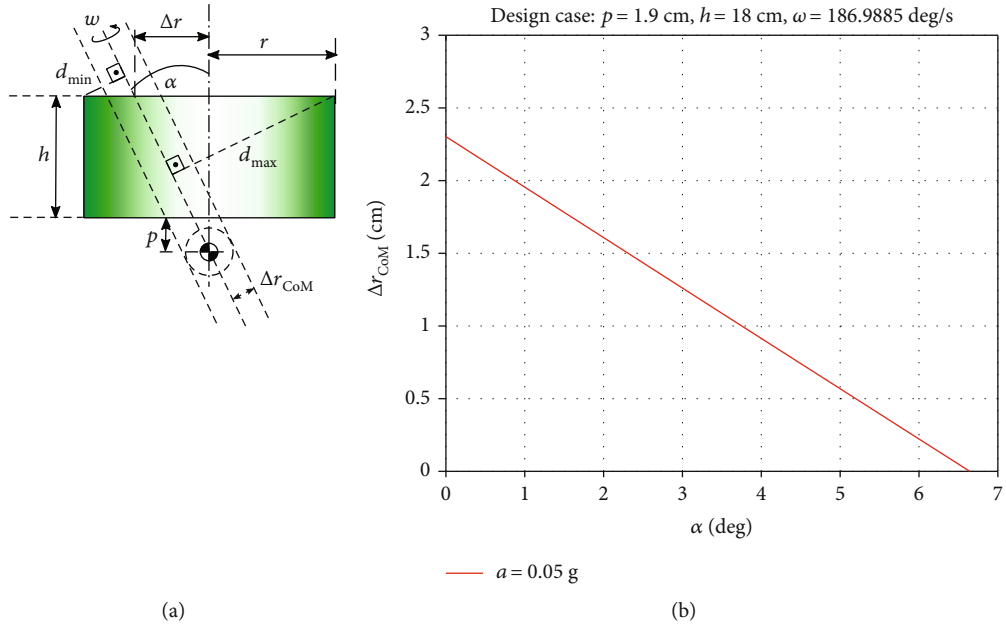

Figure 4: Payload compartment geometry and requirements on CoM offset and major moment of inertia axis angle deviation.

was violated. The analysis results of the SM CAD model differed from the MPM results.

To ensure compliance of the FM with the requirements, a test and trimming strategy was defined which contains the following measures: first, MPM of FM in different integration statuses; second, extensive CAD model refinement; third, a mathematical model was designed and verified; fourth, analysis of possible trimming measures and their effects. The mass property testing timeline is shown in Figure 5.

In total, three FM mass property measurements were planned at different integration statuses to enable changes of the trimming measures. The first MPM took place directly after primary payload and bus compartment mating (Figure 6(a)).

After the mating of the bus and MDPS assembly, the second MPM was performed. This test was conducted with installed solar panel mass models to reduce the risk of damaging the sensitive solar arrays. Two configurations were tested: deployed (Figure 6(b)) and stowed (Figure 6(c)).

The third MPM served as an acceptance test. Several launch delay announcements were the reason for the time gap in-between the second and third MPM. As satellite configuration differences existed between test configurations and launch and on-orbit configuration, further analysis was necessary.

CAD model refinement was performed consistently and especially after each ICD update or FM component incoming quality inspection during which masses were measured. Harness and attachment components were modelled in detail.

Possible locations for trim masses and also other trimming possibilities were searched within the satellite CAD model. As FM structure was already in production and intake, the definition of attachment points exclusively foreseen for trim masses was not possible. Therefore, trim mass locations exhibiting enough space and attachment points had to be searched. Their usability had to be agreed with the structure subsystem engineer as additional stiffening was also not possible.

3.1. Mathematical Model. A mathematical model was programmed in Matlab to allow for further analysis possibilities. The mathematical model is divided into three main parts: database, calculation, and analysis.

Within the database, mass properties of measurement results and CAD analysis data are stored. This includes mass, CoM, and MoI of assemblies and components. The database was continuously expanded and updated, e.g., when new measurement results were available.

Mass properties of every desired satellite configuration can be computed within the calculation part. The starting point for each calculation can be either CAD data, measurement results, or results of preceding analyses. Components can be added and subtracted by applying user-defined functions which compute mass, CoM, and MoIs of the resulting assembly.

In the analysis part, the direction cosine matrix (DCM) and the principal MoIs are calculated. The angle deviation of the spin axis to spacecraft's Z-axis is computed using the DCM as input. Based on the principal MoIs, MoI ratios like M_2/M_1 are calculated.

All test configurations differ from the relevant mission configurations, e.g., a separation mechanism simulator is used during mass property testing whereas in flight configuration only the upper part of the separation system remains on the satellite. The mathematical model is used for test predictions, test evaluation, analysis of trimming measures, and calculation of all relevant satellite configurations. After each test, the mathematical model is refined by updating the model's database, the analysis is repeated, and trimming measures are reviewed.

3.2. Verification Strategy. Test cases generated in CATIA are used to validate the mathematical model. This is done to exclude any programming issues. In these test cases, the difference between Matlab script and CATIA analysis results is of very small extent (e.g., $10^{-12}\,\mathrm{kgm}^2$) compared to satellite MoIs and can be neglected.

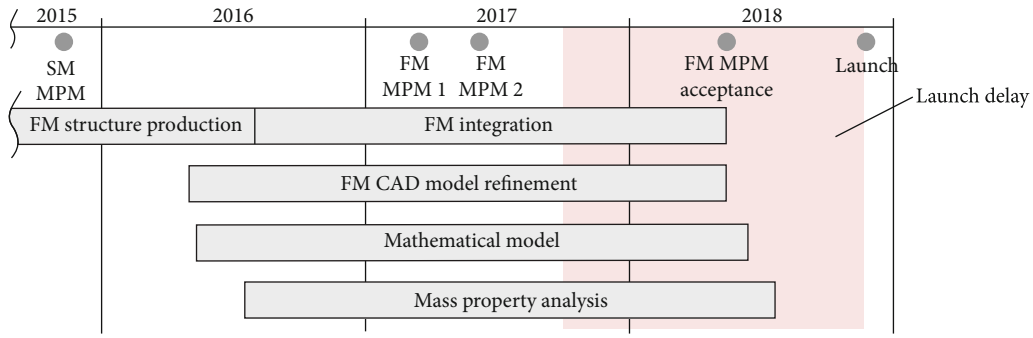

Figure 5: Mass property testing timeline.

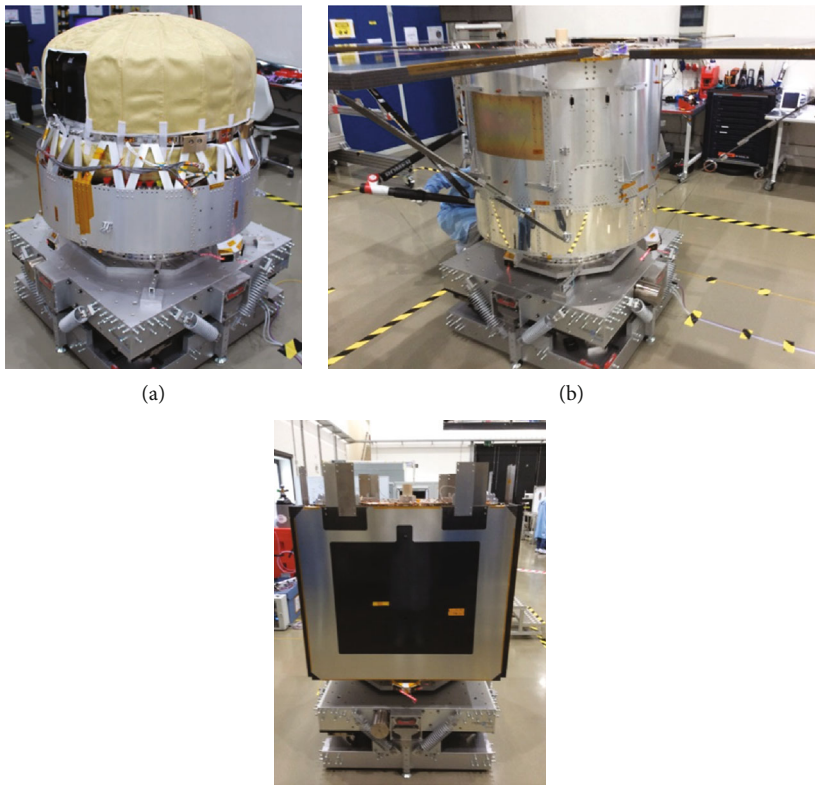

Figure 6: (a) FM MPM 1, (b) FM MPM 2 deployed configuration, and (c) FM MPM 2 stowed configuration.

The postprocessing of test measurement data is done with this mathematical model to calculate mass properties for the relevant satellite configurations, especially for nominal launch and flight configurations. The calculation results are the basement for the compliance judgement.

3.3. Trimming Measures. After a first CAD model refinement and mathematical model set-up, trimming measures could be analysed.

As a first step, the rotation of P/L1 installation direction was considered as this would not result in a higher satellite mass. A rotation around Z-axis of the P/L1 leads to an alteration of the deviation moment I_{XY} and therefore to an adjustment of the two minor MoIs. As the AOCS is all magnetic, the magnetic behaviour of each equipment including the P/L1 was measured. The P/L1 contains pump and valve arrays with a quite strong magnetic behaviour. Magnetic torquers were installed in the vicinity of these arrays on top plate and on the cylindrical part of the MDPS. Considering the possible interaction between pumps, valves, and magnetic torquers, a rotation by 40° in clockwise direction was performed to adjust the two minor MoIs.

As second step, four different locations were identified for adding trim masses (Figure 7), each exhibiting different effects on the principal MoIs and deviation moments due to their position relative to satellite's CoM: P/L1 adapter cone, top plate, and two positions on the MDPS. The trim mass properties as well as their relative position to satellite's CoM are listed in Table 3. All trim masses are in total 5.955 kg.

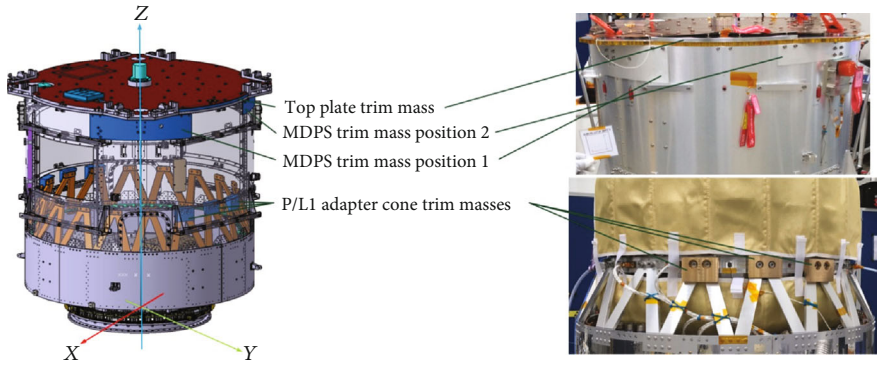

Figure 7: Trim mass locations and trim masses.

Table 3: Trim mass properties.

Position	Mass total (kg)	Material	Surface finish	ΔCoM dX	ΔCoM dY (m)	ΔCoM dZ
4x P/L1 adapter cone Typ 1	3.312 kg	RG7	None	0.000	0.000	-0.054
2x P/L1 adapter cone Typ 2	0.952 kg	RG7	None	0.000	0.000	0.004
1x top plate	0.422 kg	7075 T6	Surtec 650	0.000	0.466	0.469
1x MDPS positon 1	0.991 kg	AlMg3	Surtec 650	0.344	0.344	0.396
1x MDPS positon 2	0.278 kg	AlMg3	Surtec 650	-0.341	0.342	0.420
Sum	5.955 kg					

The P/L1 adapter cone trim masses are located close to the $\pm Y$-axis, adjust one of the minor principal MoIs and have no effect on deviation moments as their CoM lays nearly in the XY-plane of satellite's CoM.

The top plate trim mass is located on the $+Y$-axis and is used for the adjustment of one of the minor principal MoIs and of deviation moment I_{YZ}.

Two positions for trim masses on the MDPS increase all principal MoIs to nearly the same extent and have therefore negligible effect on the adjustment of those. Due to their position, both trim masses have a high effect on the adjustment of all deviation moments. MDPS trim mass position 1 is located in the first quadrant of the XY-plane. It decreases all deviation moments. Trim mass position 2 is located in the second quadrant. It increases I_{XY} and I_{XZ} and decreases I_{YZ}.

3.4. Test Facilities. The test rigs 450F and 25K were used for the mass property acceptance measurement campaign at the integration laboratory of the DLR Institute of Space Systems in Bremen. Full system measurements were performed on the 450F being capable of measuring test objects up to 450 kg, whereas solar panel measurements were performed on the 25K being capable of measuring test objects up to 25 kg.

Figure 8 shows the basic architecture of a type F machine. The test object rests on a stiff horizontal platform plate that is supported at its center by a frictionless air bearing with five degrees of freedom (DoFs). The platform is also linked to the support by multiple coil springs. As a result, the platform is capable of free vibrations with five vibration modes, typically well below 2 Hz.

After an initial excitation by hand, load cells connected to eight of the springs capture the free vibration signals for about 30 seconds. The software then computes the full mass properties, mass, CoM, and MoI, based on the five unscaled mode shapes and natural frequencies contained in the signals and based on a 5×5 stiffness matrix representing the coil

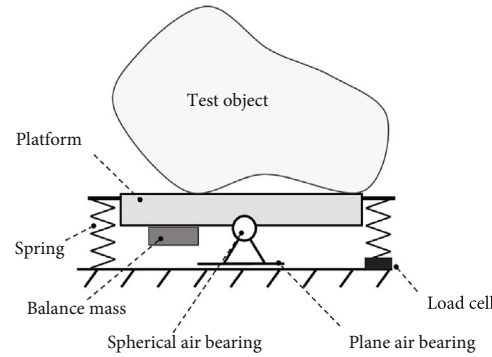

Figure 8: Components of the 450F device.

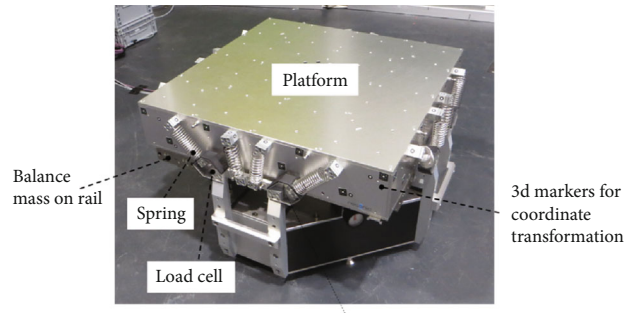

Figure 9: Components of the 450F device.

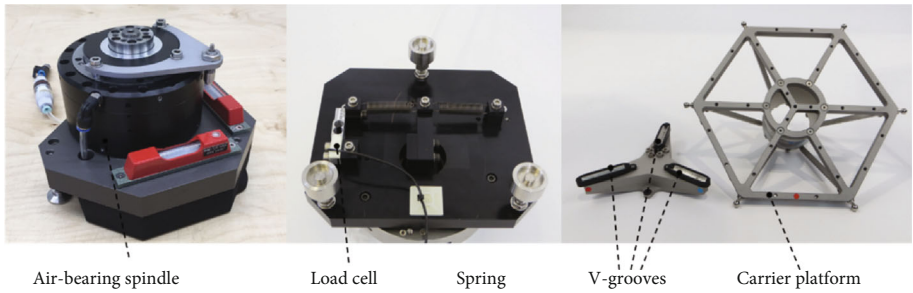

Figure 10: Components of the 25K device.

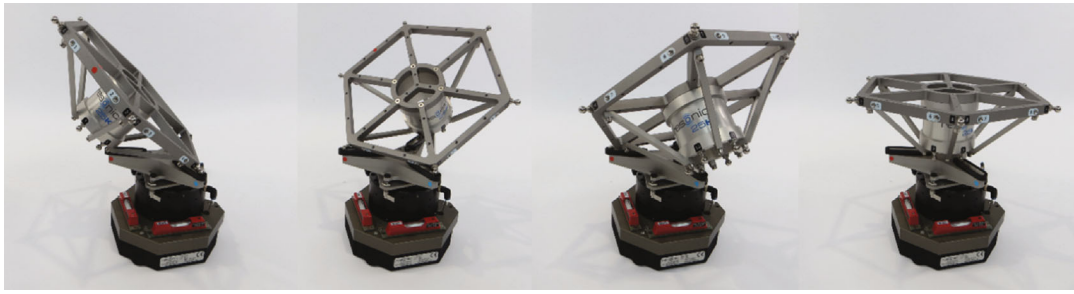

Figure 11: Different positions of the carrier platform on the air-bearing pendulum.

springs [5]. The stiffness matrix is part of the machine data and is updated in a calibration procedure every year.

For improved accuracy, the test object mass is measured by conventional scales and treated as a known quantity. Likewise, the horizontal CoM location is derived before the measurement from the combined mass and CoM of balance masses. The balance masses are installed on linear rails on four sides of the platform (Figure 9), and their positions are adjusted until the platform position is perfectly horizontal. The software computes the balance mass CoMs based on the positions measured by linear encoders.

Due to the horizontal platform and small accelerations, many test objects can be placed directly on the measurement platform without the help of fixture components. When fixtures are used, their mass properties are measured after the test object has been removed and subtracted from the overall result. The overall result is transformed into test object coordinates based on a 3d measurement of the test object position on the platform, using photogrammetry of 3d measurement arms.

Figure 10 shows the basic architecture of a type K device. A 1-DoF torsion pendulum is formed by a vertical air-bearing spindle connected to a lever and two coil springs. After starting the oscillation by hand, the natural frequency is derived from the signal of a load cell installed between the support and one of the two springs.

The test object is mounted to a carrier platform and successively placed on the pendulum in 24 different positions, varying both the test object orientation and its distance from the pendulum axis. Varying the distance is a prerequisite for measuring the CoM. The need to lift the test object by hand limits the technology to lightweight objects, ideally below 25 kg.

The interface between the carrier platform and the pendulum uses a well-known principle for highly repeatable positioning tasks: three balls on the carrier platform fit into three radial v-grooves on the pendulum. The carrier platform has a total of 12 ball studs that can be placed in the v-grooves in 24 different combinations, as shown in Figure 11.

The software derives the full inertia tensor and the three CoM coordinates from the oscillation frequencies measured first for the test object and then for the empty platform and fixtures [6]. In addition, the algorithm uses the known locations and orientations of the pendulum axis relative to the platform coordinate system. These positions are measured only once after the device has been assembled for the first time, using a 3d measurement arm.

3.5. Mass Property Acceptance Measurement Campaign. In the frame of the mass property acceptance measurement campaign, two of four solar panels as well as three different satellite configurations were measured: deployed, bus, and stowed. The test and integration flow is shown in Figure 12. The measured quantities of interest were the whole set of mass properties: mass, CoM, and MoI, in order to evaluate if the requirements were met or not. The duration of the whole MPM acceptance campaign was less than five working days including integration effort and was performed at the integration laboratory of the DLR Institute of Space Systems in Bremen.

The configuration of all tests differed to some extent to launch or on-orbit configuration; differences are shown in Table 4. Test configurations are listed on the left side, and launch and flight configurations are on the right side. The relevant components are shown in Figure 13.

Measurements were performed using the 25K and the 450F. The 25K with a carrier platform was used for solar panel measurements, and the 450F was used for full system measurements.

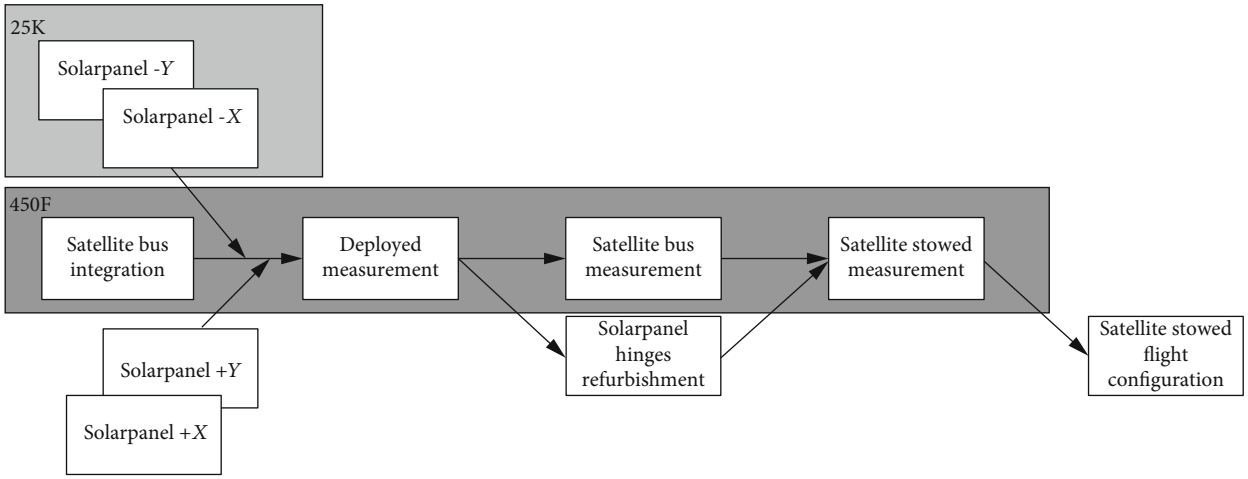

Figure 12: Test and integration flow.

Table 4: Configuration differences between test and launch or on-orbit configuration.

Component/configuration	Test			Launch		Flight	
	Deployed	Bus	Stowed	Stowed	Stowed	Deployed	Failure case
Solar panels	Deployed	na	Stowed	Stowed	Stowed	Deployed	Mixed
Tape springs	Deployed	na	Stowed	Stowed	Stowed	Deployed	Mixed
Hinge brackets	X	na	X	X	X	X	X
Hinge fasteners	X	na	X	X	X	X	X
Solar panel support arm	Deployed	Stowed	Stowed	Stowed	Stowed	Deployed	Mixed
Transition ring	X	X	X	X	na	na	na
Separation mechanism	Simulator	Simulator	Simulator	X	Separated	Separated	Separated
MLB harness	na	na	na	X	X	X	X
Acceleration sensor harness	X	X	X	Shortened	Shortened	Shortened	Shortened

Deployed = in deployed configuration; stowed = in stowed configuration; X = built-in in nominal configuration; na = not built-in; simulator = mass dummy; separated = only upper half of separation mechanism; shortened = respective harness shortened; mixed = mix of different configuration statuses.

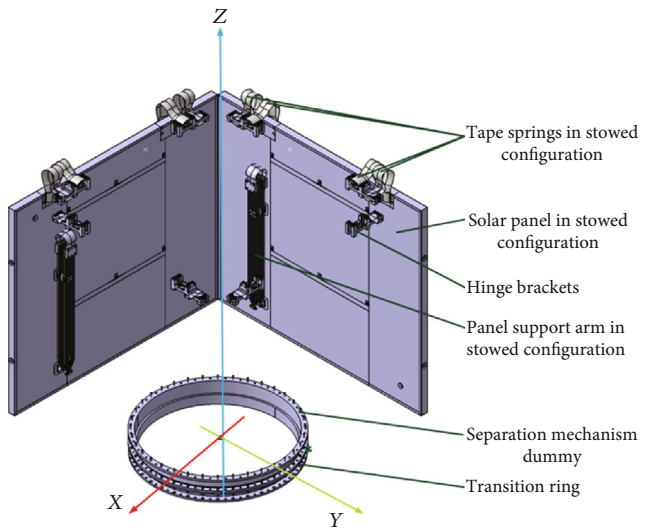

Figure 13: Configuration differences to launch and flight configurations—relevant components.

First, mass property measurement of two of four solar panels was performed (Figure 14(b)). Due to the high sensitivity of the test rig, a tent was used to exclude any influence by the integration lab air-conditioning system or by engineers walking by.

The solar panels were integrated into the system in deployed configuration afterwards, and the satellite mass properties of the deployed configuration were determined (Figure 14(a)). Integration lab air-conditioning system was regulated to a minimum to reduce air effects on the measurement results.

Then, the solar panels as well as the solar panel MGSE were deintegrated, and a mass property measurement of the satellite bus was performed. After refurbishment of the tape springs, the solar panels were reintegrated in stowed configuration and the mass property measurement of the satellite in stowed configuration was conducted (Figure 15). After the integration of the solar panels, the satellite was in flight configuration except for the launch adapter interface which was installed at the launch complex.

In between the measurements of the different configurations, zero measurements were performed to subtract out measurement platform and any MGSE.

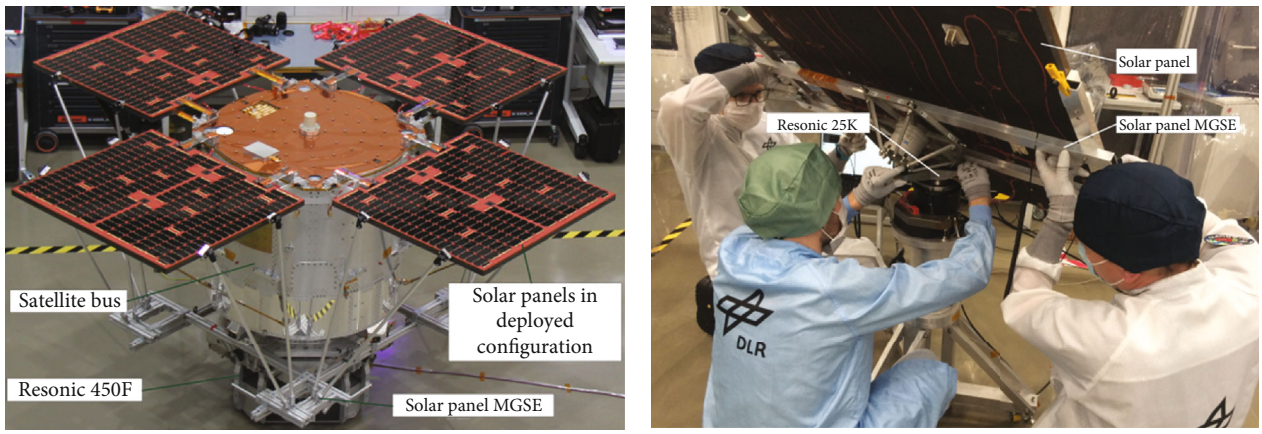

(a) (b)

Figure 14: Mass property measurement of the satellite in deployed configuration and of solar panels.

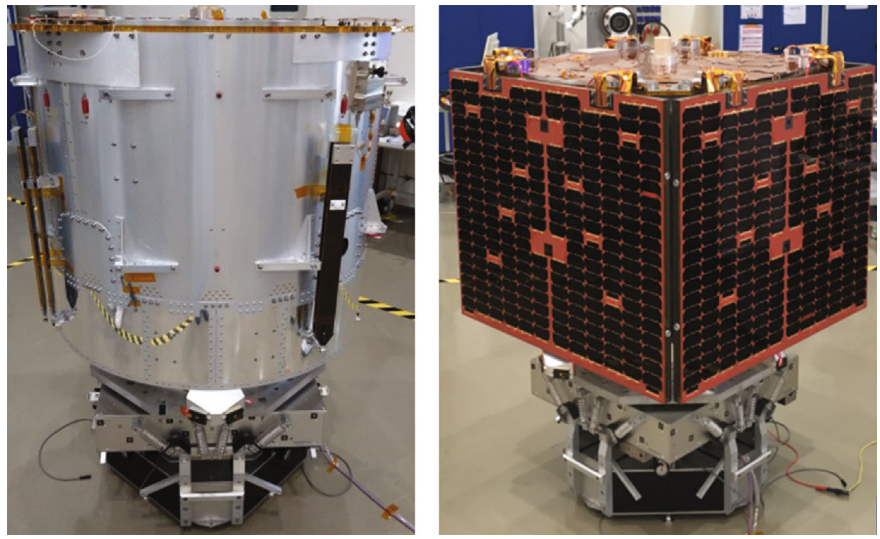

Figure 15: Mass property measurement of the satellite bus and satellite in stowed configuration.

4. Results

Hereafter the acceptance test campaign results are presented which are the basis for the succeeding analysis and compliance judgment.

4.1. Accuracy Analysis. In Resonic's experience, deriving measurement uncertainties from known uncertainties of input quantities is unreliable for simultaneous measurements of full mass properties. For obvious inputs like sensor signals, sampling rates, and geometry data, reasonable uncertainty values can be obtained from datasheets and assumptions about the statistical distributions (usually normal or uniform). By contrast, factors like the device stiffness, sensor cross-sensitivities, friction, various temperature effects, and local vibration modes of springs are very difficult to quantify, in particular for multi-DoF machines like 450F. But most importantly, there is always a risk of being unaware of an important factor.

For these reasons, the measurement uncertainties for mass properties are evaluated based on reference measurements. The reference objects are composed of precision steel cylinders whose *true* mass properties can be derived from the cylinder mass, geometry, and position in 3d space. By arranging different cylinders on tall carrier frames, any variety of mass properties, like different masses, MoIs, and CoM positions, can be generated, and the accuracy of the device in measuring these mass properties can be tested. For each reference measurement, a true value and absolute measurement error as well as a relative measurement error are reported. Based on this data, mean values as well as standard deviations of the relative measurement error were calculated for masses between 100 kg and 400 kg. As Eu:CROPIS also contains water and is, compared to the calibration masses, more susceptible to air effects, an additional safety factor of three was introduced. In Table 5, the measurement uncertainties including the additional safety factor are listed. These percentage values are related to the maximum MoI measured.

4.2. Analysis Results. Postprocessed test results from the mass property measurement acceptance test campaign were used

Table 5: Measurement uncertainties on 3σ-niveau.

I_{XX} (%)	I_{YY} (%)	I_{ZZ} (%)	I_{XY} (%)	I_{XZ} (%)	I_{YZ} (%)
0.7359	0.7335	0.6956	0.3137	0.7744	0.6159

for the requirement verification. As stated before, test configurations differed to relevant launch and flight configurations. Mass properties of these components (Table 4) were obtained using the CAD model.

As only the $-X$ and $-Y$ solar panels were tested, the results were extrapolated to the $+X$ and $+Y$ panels. The CoM of the $+X$ and $+Y$ panel was approximated by using the mean value of the tested panels $-X$ and $-Y$:

$$\mathrm{CoM}_{+X,+Y} = \frac{\mathrm{CoM}_{-X} + \mathrm{CoM}_{-Y}}{2}. \quad (1)$$

The inertia values of the untested panels were calculated by using the test results of the $-X$ and $-Y$ panels. Both solar panel test results were divided by their respective panel mass and were averaged. The averaged value was then multiplied with the mass of the untested panels:

$$I_{+X,+Y} = \frac{(I_{-X}/m_{-X}) + (I_{-Y}/m_{-Y})}{2} * m_{+X,+Y}. \quad (2)$$

On system level, three configurations were tested. To prove measurement data consistency, each configuration was calculated into one another. The stowed and bus configuration can be mathematically transformed well into one another. But the transformation of both stowed and bus configuration into deployed configuration leads to differences in I_{XX}, I_{YY}, I_{XZ}, and I_{YZ}. Therefore, the test conductor ran a dedicated analysis to investigate the reasons for these differences. Following impacts had influenced the deployed test results:

(i) *Atmospheric Effects*: In deployed configuration, the relevant area was approximately five times higher than in stowed or bus configuration. This leads to a mass loading effect which influenced measurement results

(ii) *Water Effects*: Water tanks were installed inside PL-1. Even if these tanks were nearly completely filled, sloshing could occur. This effect could occur in all three satellite configurations measured and lead to a motion damping

(iii) Elastic movements of solar panel and its mounting in deployed configuration

In this analysis, the measurement time was optimized for the deployed and bus configurations; measurement time of stowed configuration remained unchanged. Using these optimized test results, the mathematical transformation of bus and stowed configurations into deployed configuration varied only in terms of I_{XX} and I_{YY}. This is a hint that atmospheric effects and also elastic movements of the solar panels had influenced the deployed test results. Therefore, the bus and stowed test results were the basis for the calculation of all other possible satellite configurations.

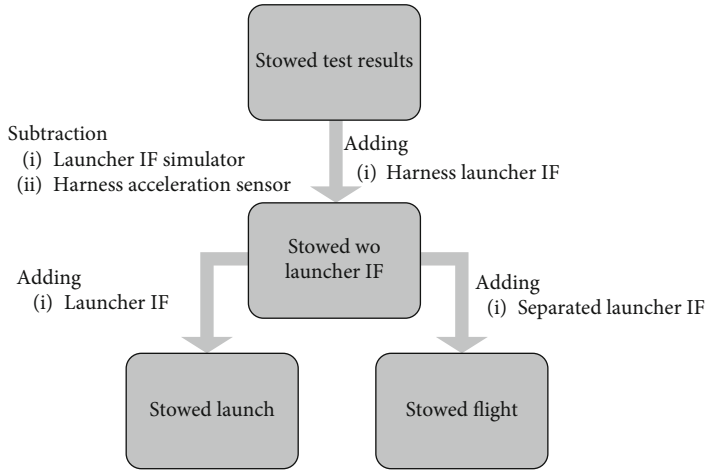

Figure 16: Calculation of stowed launch and flight configuration.

Table 6: Mass, CoM, and MoI of stowed launch and flight configuration.

		Stowed launch	Stowed flight
Mass (kg)	m	233.77	226.6
CoM (mm)	X	1.9	2.0
	Y	5.5	5.1
	Z	370.2	385.3
MoI (kgm^2)	I_{XX}	34.868 ± 0.259	32.850 ± 0.259
	I_{YY}	35.110 ± 0.258	33.131 ± 0.258
	I_{ZZ}	35.333 ± 0.245	34.690 ± 0.245
	I_{XY}	−0.053 ± 0.110	−0.052 ± 0.110
	I_{XZ}	0.077 ± 0.273	0.082 ± 0.273
	I_{YZ}	0.150 ± 0.217	0.111 ± 0.217

Table 7: Stowed flight configuration analysis results.

	Stowed flight
M_1 (kgm^2)	32.835
M_2 (kgm^2)	33.134
M_3 (kgm^2)	34.702
Angle deviation (°)	4.6
M_{max}/M_{min} (-)	1.057
M_2/M_1 (-)	1.009

4.3. Calculation of Stowed Launch and Flight Configuration. The calculation of the stowed launch and flight configurations was based on stowed test results. First, the launcher interface simulator and the harness acceleration sensor were subtracted out, and the harness of the launcher IF was added on. The complete launcher IF was added for calculation of the stowed launch configuration, whereas for the stowed flight configuration, only the separated upper part of the launcher IF was added (Figure 16). The resulting mass, CoM, and MoI are listed in Table 6.

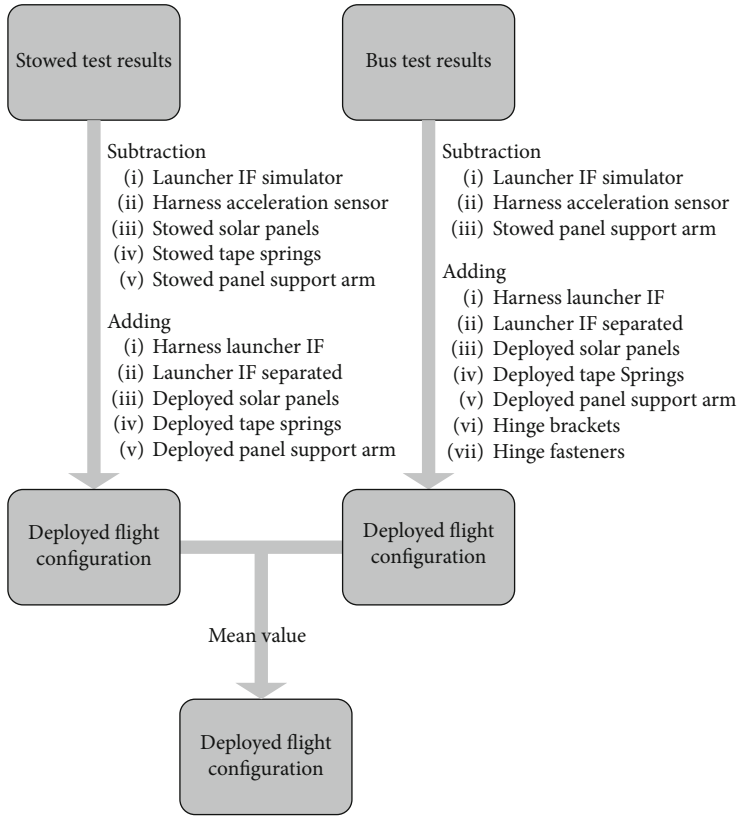

Figure 17: Calculation of deployed flight configuration.

The analysis shows a compliance of the stowed launch configuration in terms of total mass (RE-LP-1), CoM lateral (RE-LP-2), and axial offset (RE-LP-3).

The stowed flight configuration is compliant in terms of maximum principal moment magnitude (RE-AOCS-2) and rotation axis (RE-AOCS-1) (Table 7).

4.4. Calculation of Deployed Flight Configuration. As the measurement results of the deployed configuration could not be used as a basis for the compliance judgement of the deployed flight configuration, a different approach was selected.

Bus and stowed test results were used as basis for the calculation of the deployed flight configuration. The calculation path is shown in Figure 17. The deployed result of bus and stowed configurations were averaged. The mass, CoM, and MoI are listed in Table 8.

In Table 9, the principal MoIs, the angle between spin axis, and SCF Z-axis and the corresponding principal MoI ratios are listed for the deployed flight configuration considering lower and upper bound. Each column represents one dataset.

The analysis shows a compliance of the deployed flight configuration in terms of spin axis (RE-AOCS-1), maximum principal moment magnitude (RE-AOCS-2), the ratio of the major principal MoI to the minor principal MoI (RE-AOCS-3), and the ratio of the two minor MoIs $M_{\max}/M_{\min}$ (RE-AOCS-4).

The angle between spin axis and SCF Z-axis is higher than the specified 5° for the upper limit (RE-PL-1 and RE-AOCS-5), but below its limit for the lower bound and mean values. The amount of this exceedance is relatively small: 5.6° to

Table 8: Deployed flight configuration.

		Deployed flight—mean
Mass (kg)	m	226.62
CoM (mm)	X	1.8
	Y	5.0
	Z	419.6
MoI (kgm^2)	I_{XX}	43.332 ± 0.259
	I_{YY}	43.541 ± 0.258
	I_{ZZ}	48.908 ± 0.245
	I_{XY}	-0.053 ± 0.110
	I_{XZ}	0.076 ± 0.273
	I_{YZ}	0.194 ± 0.217

Table 9: Deployed configuration analysis results.

	Deployed flight		
	Min	Mean	Max
M_1 (kgm^2)	42.978	43.317	43.565
M_2 (kgm^2)	43.371	43.548	43.773
M_3 (kgm^2)	48.670	48.916	49.207
Angle deviation (°)	-2.02	2.19	5.66
$M_{\max}/M_{\min}$ (-)	1.133	1.129	1.13
M_2/M_1 (-)	1.009	1.005	1.005

5.0°. Assuming a Gaussian distribution of the measurement error, the probability of this exceedance is about 1%.

4.5. Failure Case Mass Properties. In addition to the calculation of the three nominal configurations, 14 failure case configurations were calculated. In each failure case configuration, at minimum one solar panel has not deployed and remains in stowed configuration. The analysis shows that in nearly all configurations, the major principal MoI is I_{ZZ}, in only two configurations, this is not the case. Nevertheless, in all failure case configurations, the angle deviation between the principal axis and the Z-axis is above 21.4° and also the ratio of the two minor MoIs is far above its 5% limit.

4.6. Comparison with On-Orbit Data. Values for the DCM between body-fixed and principal axis frame became available after launch. The value for the angle deviation of the principal axis and body-fixed Z-axis was 1.92° which was below the calculated mean value of 2.19° and within the calculated limits.

5. Conclusion

This paper presents the mass property trimming campaign of DLR's first compact satellite mission Eu:CROPIS launched in December 2018.

The spin-stabilized Eu:CROPIS satellite provides artificial gravity for its primary and secondary payloads. Therefore, mass properties have to be within certain limits and also to be known with high certainty. As the structural model does not comply with most of the requirements, mass property trimming strategy is set up for the flight model. Nine trim masses are designed for satellite mass property adjustment. The complete FM trimming campaign is described alongside with the acceptance results for relevant flight configurations. On-orbit data show a very good agreement with the presented analysis results.

Finally, it can be stated that the trimming strategy proves its effectiveness, so that this approach will be used in the satellite missions to be followed.

Abbreviations

AOCS: Attitude and Orbit Control System
BSL: Biosafety level 1
CAD: Computer-aided design
CATIA: Computer-aided three-dimensional interactive application
CoM: Center of mass
DCM: Direction cosine matrix
DLR: Deutsches Zentrum für Luft- und Raumfahrt e.V. (German Aerospace Center)
DoF: Degree of freedom
Eu:CROPIS: Euglena Combined Regenerative Organic Food Production in Space
FM: Flight model
GMOs: Genetically modified organisms
ICD: Interface control document
M_1-M_3: Principal moments of inertia
Matlab: MATrix LABoratory
MDPS: Micrometeroid and Debris Protection Shield
MGSE: Mechanical ground support equipment
MLB: Motorized light band
M_{max}: Maximum principal moment
M_{min}: Minimum principal moment
MoI: Momentum of inertia
MPM: Mass property measurement
NASA: National Aeronautics and Space Administration
P/L1: Primary payload
Powercell: NASA payload on Eu:CROPIS
RAMIS: Radiation Measurement in Space
SCF: Structural coordinate frame
SCORE: SCalable On-boaRd computer
SM: Structural model
SSO-A: Sun synchronous orbit—mission A.

Data Availability

The data used to support the findings of this study are included within the article.

Conflicts of Interest

The authors declare that there is no conflict of interest regarding the publication of this paper.

References

[1] S. Kottmeier, C. Hobbie, F. Orlowski-Feldhusen et al., "The Eu:CROPIS Assembly, Integration, and Verification Campaigns: Building the First DLR Compact Satellite," in *69th International Astronautical Congress 2018*, pp. 1–5, Bremen, Germany, 2018.

[2] T. Delovski, C. Düvel, F. Greif et al., "Eu:CROPIS AIV Program: Challenges and Solutions for a Spin-Stabilized Satellite Containing Biology," *International Journal of Aerospace Engineering*, vol. 2019, Article ID 9190329, 20 pages, 2019.

[3] A. Heidecker, T. Kato, O. Maibaum, and M. Hölzel, "Attitude control system of the Eu:CROPIS mission," in *65th International Astronautical Congress*, Toronto, Canada, 2014.

[4] A. Heidecker, M. Schlotterer, O. Maibaum, E. Panzenböck, S. Löw, and M. Markgraf, "Magnetic Attitude Control of a Spinning Spacecraft:Flight Results and Lessons Learned from DLR's Compact Satellite Eu:CROPIS," in *12th IAA Symposium on Small Satellites for Earth Observation*, Berlin, Germany, 2019.

[5] R. Kloepper, M. Okuma, and J. Bienert, "A Compact Device for Measuring Rigid-Body Properties Based on Five Unscaled Modes," in *Topics in Modal Analysis I*, vol. 7 of Conference Proceedings of the Society for Experimental Mechanics Series, , pp. 215–224, Springer, 2014.

[6] R. Kloepper and H.-P. Groebelbauer, "A Multi-Sided Kinematic Coupling Combined with an Air Bearing," in *Proceedings of the 13th European Conference on Spacecraft Structures, Materials & Environmental Testing*, Braunschweig, Germany, 2014.